Supporting Information for

Tough, Highly Conductive and Flame-Retardant MXene/NR Films Based on Large-Size MXene for Efficient Electromagnetic Interference Shielding

Yongjie Bi [a], Yedan Ding [f], Yingfan Li [b], Jiayin Li [c], Chao Teng [c], Xiaoyan Ma *[d], Xingrong Zhang *[de], Qi Chen *[a], Hongzhen Wang *[a]

[a] College of Polymer Science and Engineering, Qingdao University of Science and Technology, Qingdao 266042, P. R. China.

[b] Carbon Fiber Engineering Research Center, School of Materials Science and Engineering, Shandong University, Jinan 250061, China.

[c] College of Materials Science and Engineering, Qingdao University of Science and Technology, Qingdao 266042, China.

[d] College of Chemical Engineering, Qingdao University of Science and Technology, Qingdao 266042, China.

[e] College of Chemical Engineering, Eco-Chemical Engineering Cooperative Innovation, Center of Shandong, Qingdao University of Science and Technology, Qingdao 266042.

[f] Sino-German College of Engineering, Qingdao University of Science and Technology，Qingdao 266042, China.

*Corresponding author. E-mail: maxiaoyan@qust.edu.cn; zhxr1984@126.com; chenqiqust@163.com; qustwhz@163.com

S1 Supplemental Experimental Procedures

Characterization. The morphology and microstructure (surface and cross-section) of NRL, MXene and nanocomposite films were observed using a cold field emission scanning electron microscope (SEM, Regulus 8100, Hitachi, Japan). The morphology and structure of MXene dispersions were further investigated by transmission electron microscopy (TEM, JEOL JEM-F200, Japan) and atomic force microscopy (AFM Bruker Dimension Icon, Germany). Zeta potential of NR, Al-$Ti_3C_2T_x$, Al-$Ti_3C_2T_x$ /NR dispersions were tested using a nanoparticle size and zeta potential analyzer (DLS, Malvern Zetasizer Nano ZS90, Japan) The identification of MAX, NR, Al-$Ti_3C_2T_x$ NR, Al-$Ti_3C_2T_x$, and Al-$Ti_3C_2T_x$/NR on XRD (Rigaku SmartLab SE, Japan). The chemical compositions of NR, AL-$Ti_3C_2T_x$, AL-$Ti_3C_2T_x$/NR nanocomposite films were analyzed by XPS (Thermo Scientific K-Alpha, USA) and FTIR spectroscopy. The mechanical properties of the prepared films were tested at room temperature using an electronic universal testing machine (KXWW-05C, Chengde Kebiao Testing Instrument Manufacturing Co., Ltd.). The samples were cut into regular long strips and the tensile speed was set at 500 mm min^{-1}. At least three similar curves were obtained for each sample to evaluate the mechanical properties.The electrical conductivity of the prepared films was analyzed by the four-probe method (ST-2258C, Suzhou Jingge Electronics Co., Ltd., probe diameter: 1.02 mm, probe spacing: 2 mm). The electrical conductivity of the prepared composites was calculated according to the following equation:where σ, t, and Rs are the electrical conductivity , thickness , and sheet resistance of the nanocomposite film, respectively.

$$\sigma = 1/(R_S \times \mathrm{t})$$ * MERGEFORMAT [1]

The electromagnetic shielding performance is measured by a（Rohde & Schwarz ZNLE18）two-port vector network analyzer in the frequency range from 8.2 to 12.4 GHz (X-band). The reflection (R), transmission (T) and absorption (A) coefficients are governed by the S parameters (S_{11}, S_{12}, S_{21}, S_{22}) of the scattered energy from the material or device.

$$R = |S_{11}|^2 = |S_{22}|^2, T = |S_{12}|^2 = |S_{21}|^2, A = 1 - R - T$$ * MERGEFORMAT [2]

In addition, the total EMI SE (SE_T), absorption (SE_A), multiple reflection (SE_M) and reflection (SE_R) efficiencies can be calculated using equations relating the A, R and T coefficients.

$$SE_A = -10\log\left(\frac{T}{1-R}\right), SE_R = -10\log(1-R), SE_T = SE_A = SE_M = SE_R$$ * MERGEFORMAT [3]

In particular, the value of SE_M is almost zero and negligible when the SE_T exceeds 10 dB, where the major reflected waves are absorbed and converted into heat inside the material. The shielding efficiency of the Al-$Ti_3C_2T_x$/NR nanocomposites, which refers to the ability to block waves, can be expressed as followed:

$$shielding\ efficiency(\%) = 100 - \left(\frac{1}{10^{SE_T/10}}\right) \times 100$$ * MERGEFORMAT

[4]

Furthermore, *SSE* and *SSE/t* are defined to eliminate the effect of thickness and density on the EMI SE of Al-$Ti_3C_2T_x$/ANF nanocomposites.

$$SSE = EMI\ SE\ /\ density = dB \cdot cm^3 \cdot g^{-1}$$ * MERGEFORMAT [5]

$$SSE\ /\ t = SSE\ /\ thickness = dB \cdot cm^3 \cdot g^{-1}$$ * MERGEFORMAT [6]

The weight loss of NR, Al-$Ti_3C_2T_x$, and Al-$Ti_3C_2T_x$/NR=10/90 films was tested by using (TGA,TA) in nitrogen atmosphere from 30°C to 800°C at a temperature increase rate of 10 °C-min^{-1}. The heat release rate and total heat release of the three films of NR, Al-$Ti_3C_2T_x$, and Al-$Ti_3C_2T_x$/NR=10/90 from 200°C to 700°C at a rate of 1 °C/s were measured by using the microcalorimeter (MCC). $Ti_3C_2T_x$/NR=10/90 were measured by using a microcalorimeter (MCC) to measure the heat release rate and the total heat release of NR, Al-$Ti_3C_2T_x$, and Al-$Ti_3C_2T_x$/NR=10/90 films from 200°C to 700°C at a rate of 1 °C/s. The macroscopic flame retardant experiments were performed with an alcohol lamp.

S2 Supplementary Figures and Tables

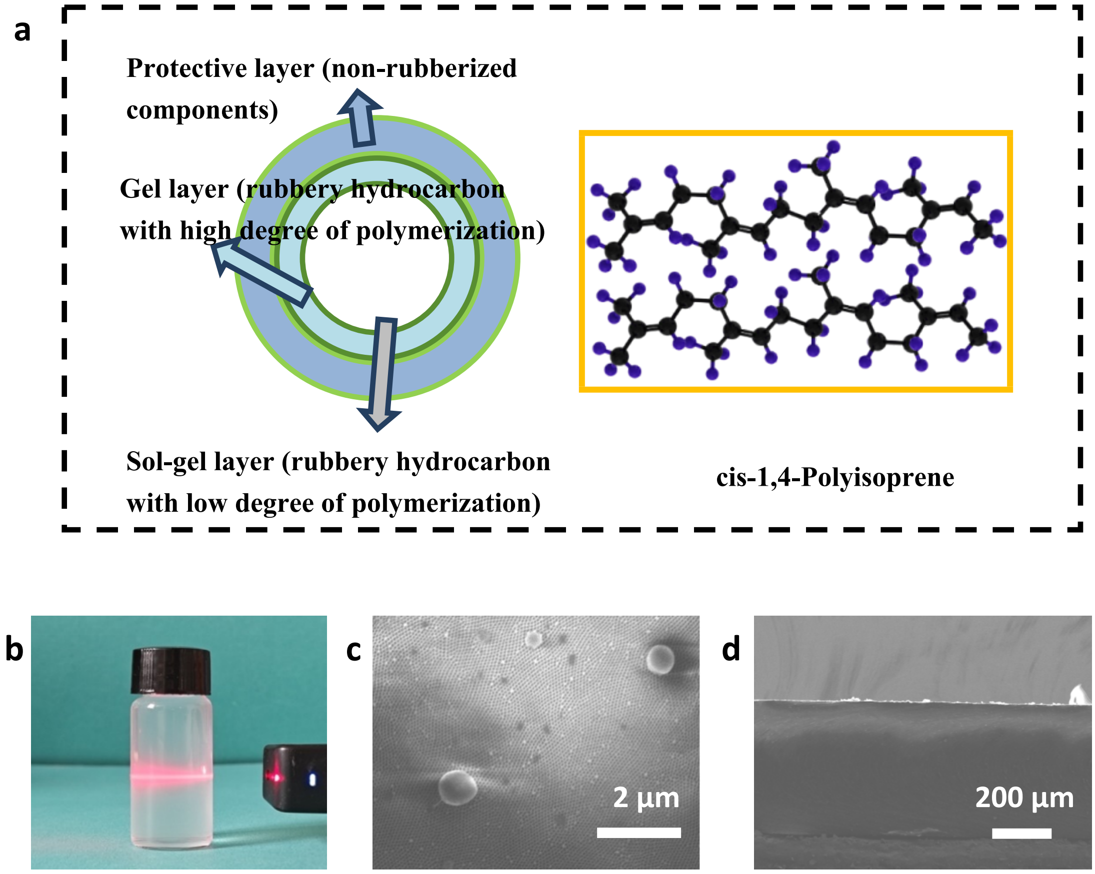

Fig. S1 a Structural composition of rubber particles. **b** Tyndall effect. **c** SEM image of NR dispersion. **d** Cross-sectional SEM image of NR film after vacuum filtration and drying.

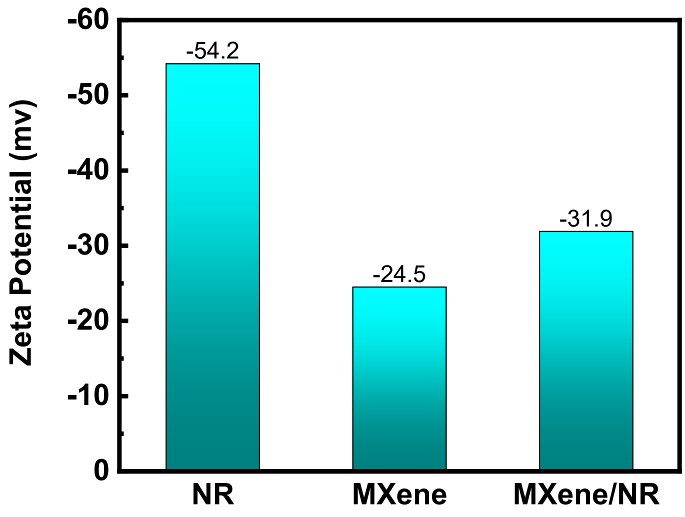

Fig. S2 Zeta potential of NR, Al-$Ti_3C_2T_x$ and Al-$Ti_3C_2T_x$/NR dispersion.

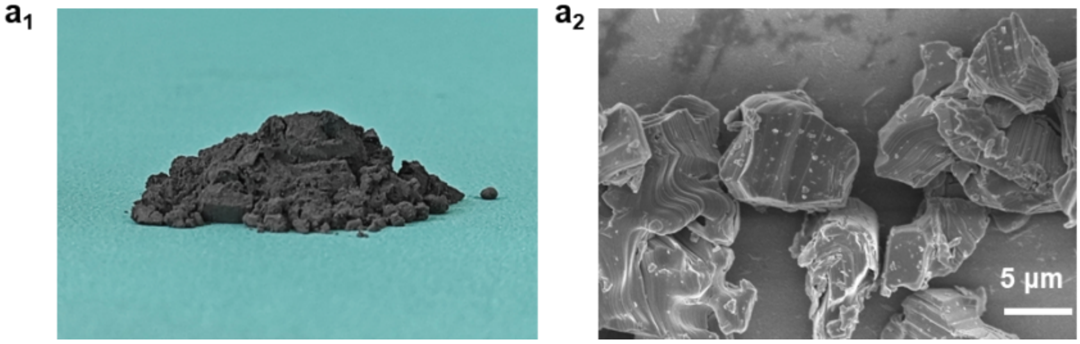

Fig. S3 a$_1$ optical photograph of MAX. **a$_2$** SEM images of MAX.

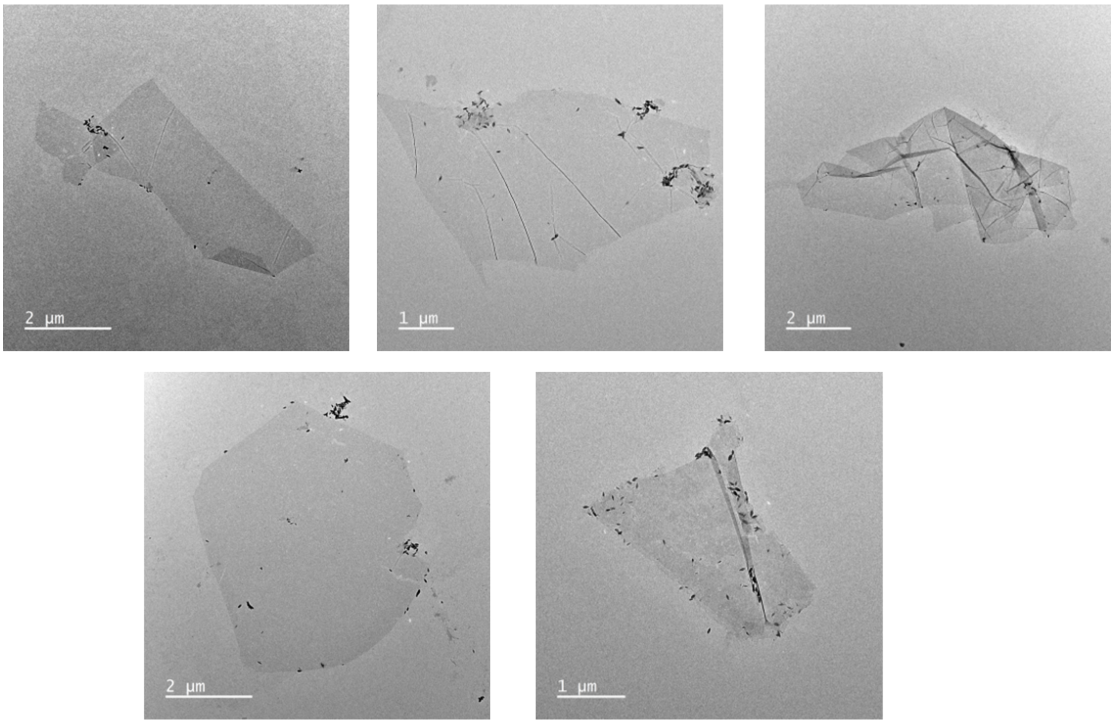

Fig. S4 TEM images of Al-$Ti_3C_2T_x$ single-layer nanosheets.

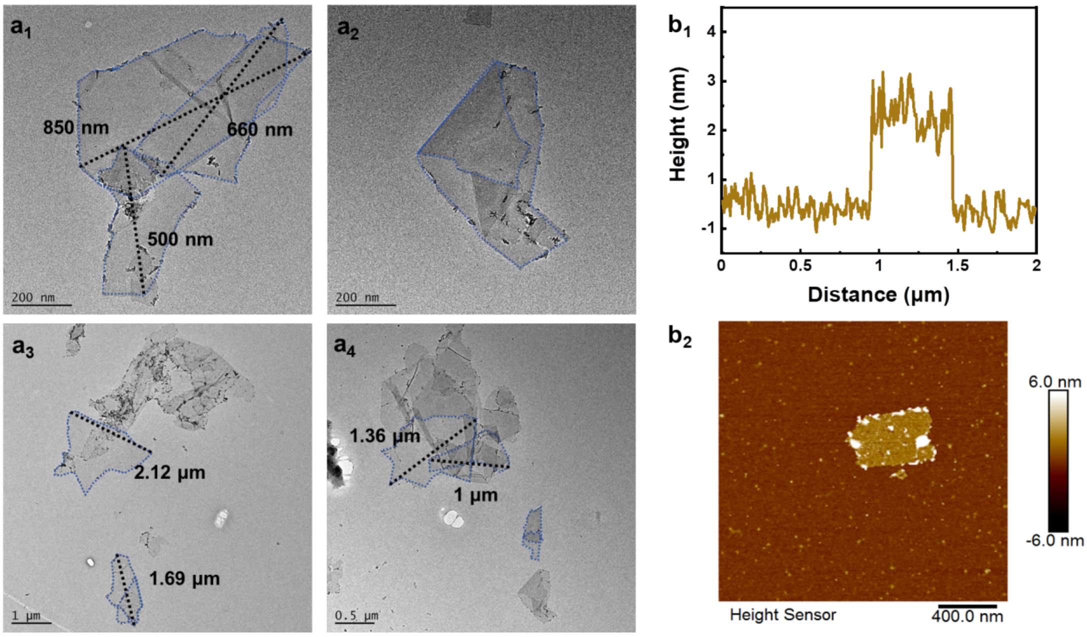

Fig. S5 TEM (**a_1-a_4**) and AFM (**b_1-b_2**) characterization and statistical results of conventional MXene nanosheets.

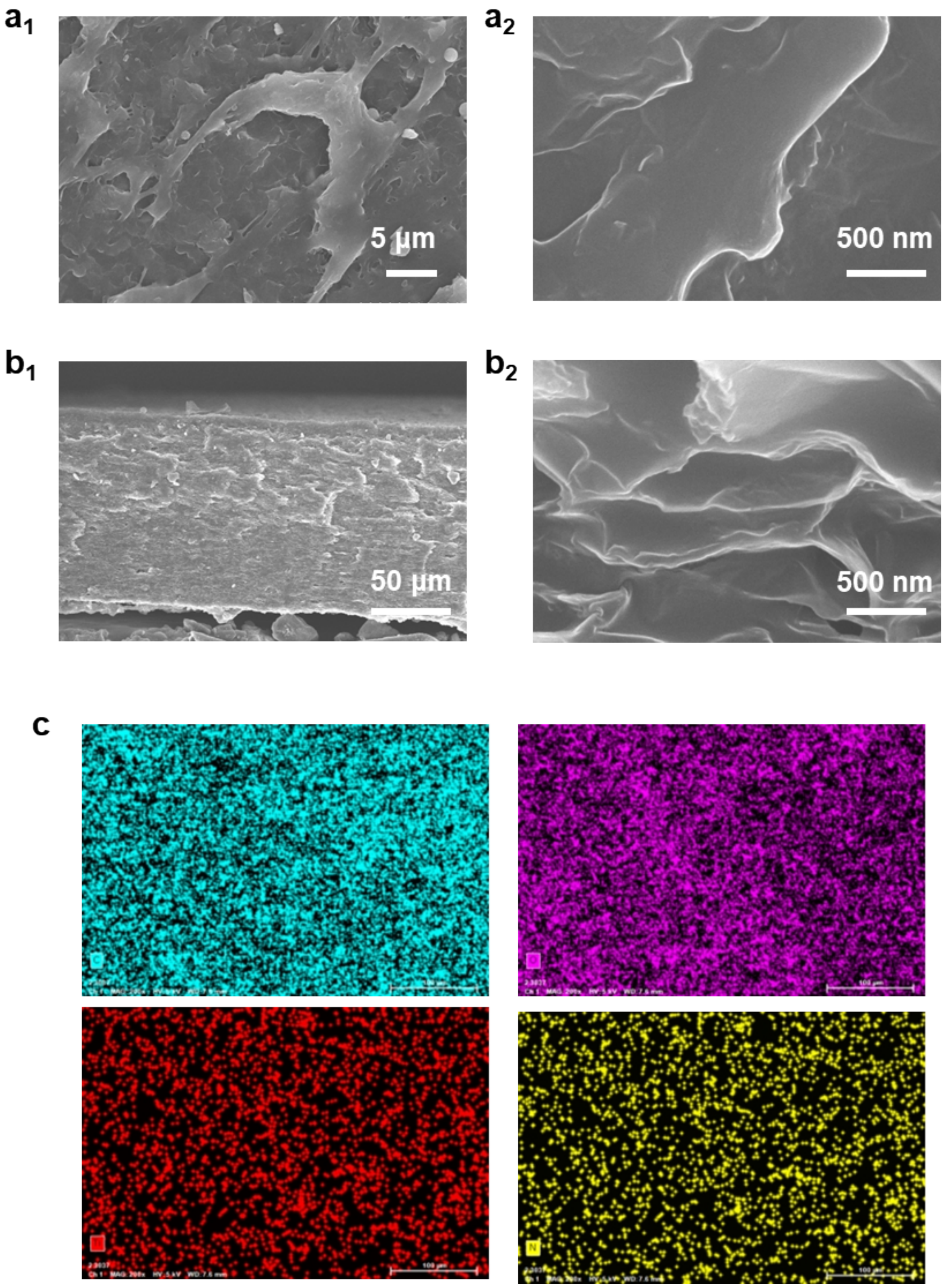

Fig. S6 (**a_1, a_2**) Surface SEM images. (**b_1, b_2**) Cross-sectional SEM images, **c** EDS mapping images of a 10 wt% Al-$Ti_3C_2T_x$/NR composite film.

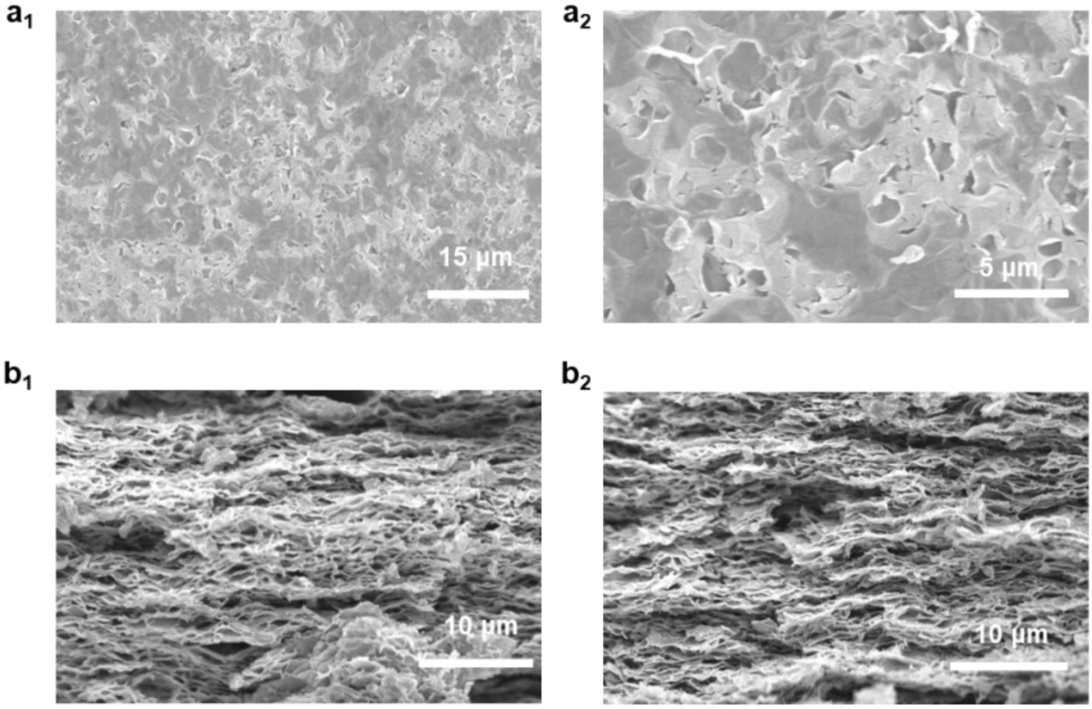

Fig. S7 (a$_1$, a$_2$) Surface SEM images. **(b$_1$, b$_2$)** Cross-sectional SEM images of a 10 wt% Al-$Ti_3C_2T_x$/NR composite film.after heat treatment.

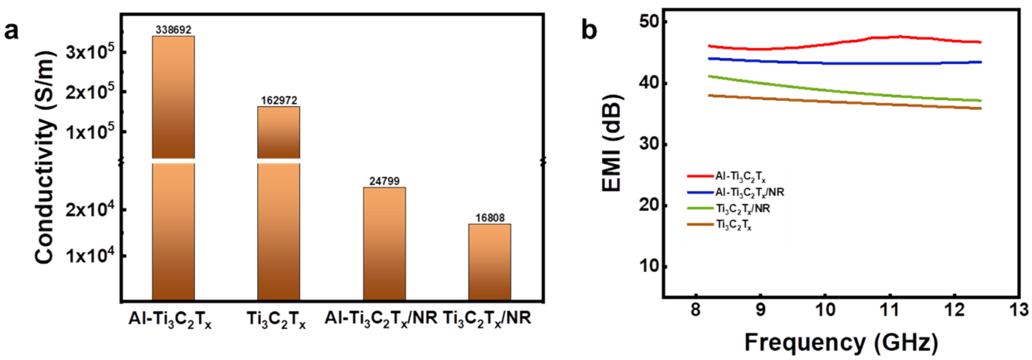

Fig. S8 Electrical conductivity (**a**) and EMI SE (**b**) of Al–$Ti_3C_2T_x$, $Ti_3C_2T_x$, and their composite films with NR.

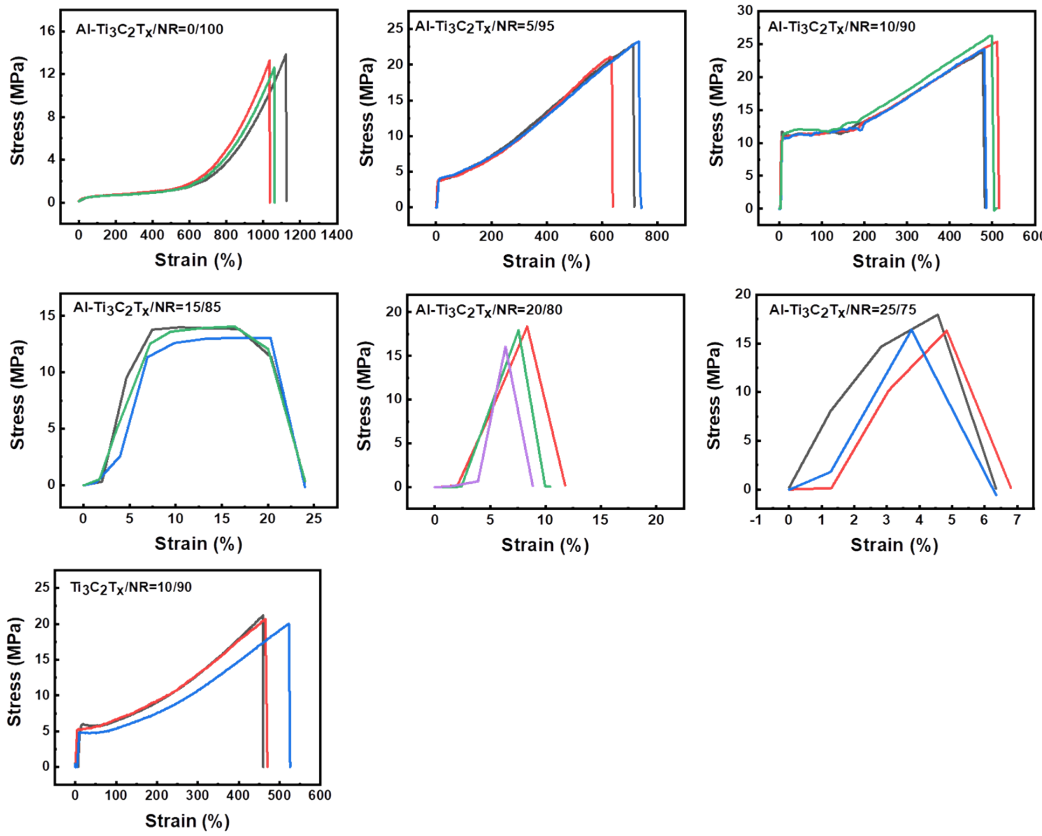

Fig. S9 Stress–strain curves of MXene/NR films with varying MXene mass ratios.

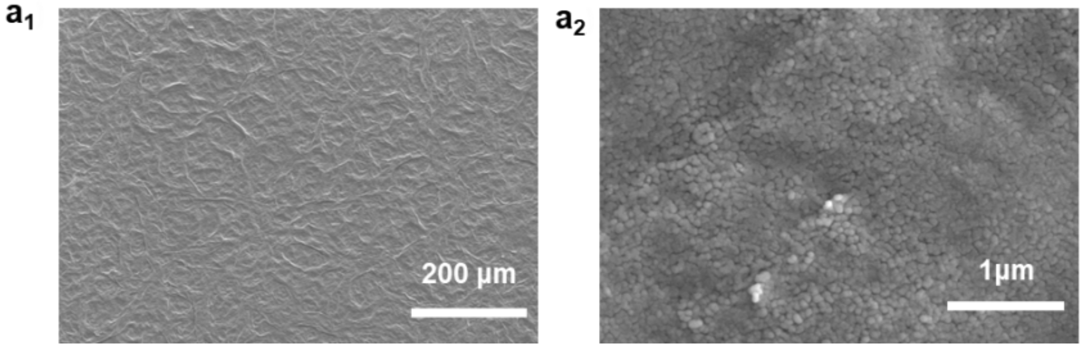

Fig. S10 (a_1, a_2) SEM images of Al-$Ti_3C_2T_x$ film after heat treatment.

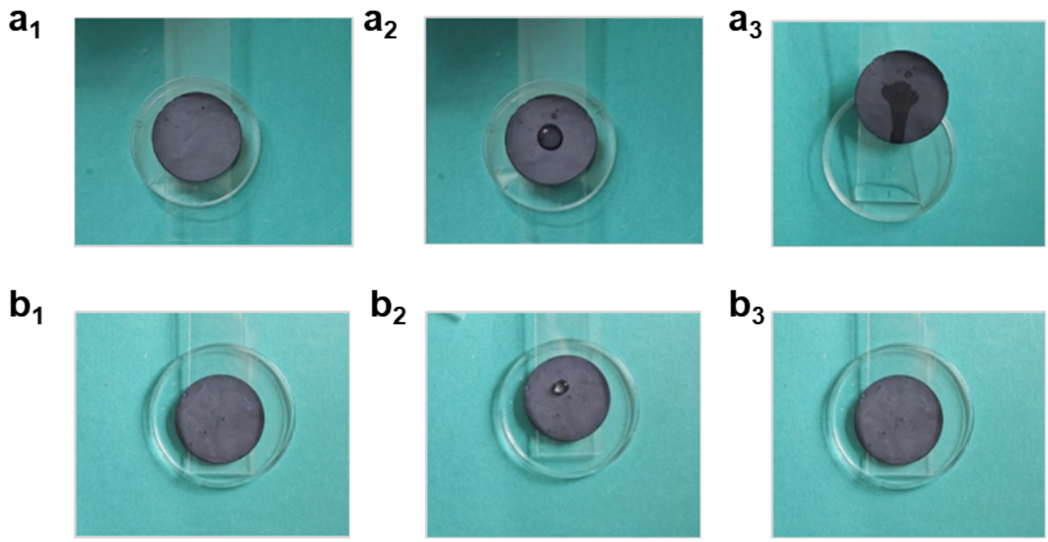

Fig. S11 Droplet test on the film before (**a**) and after (**b**) the hydrophilic modification.

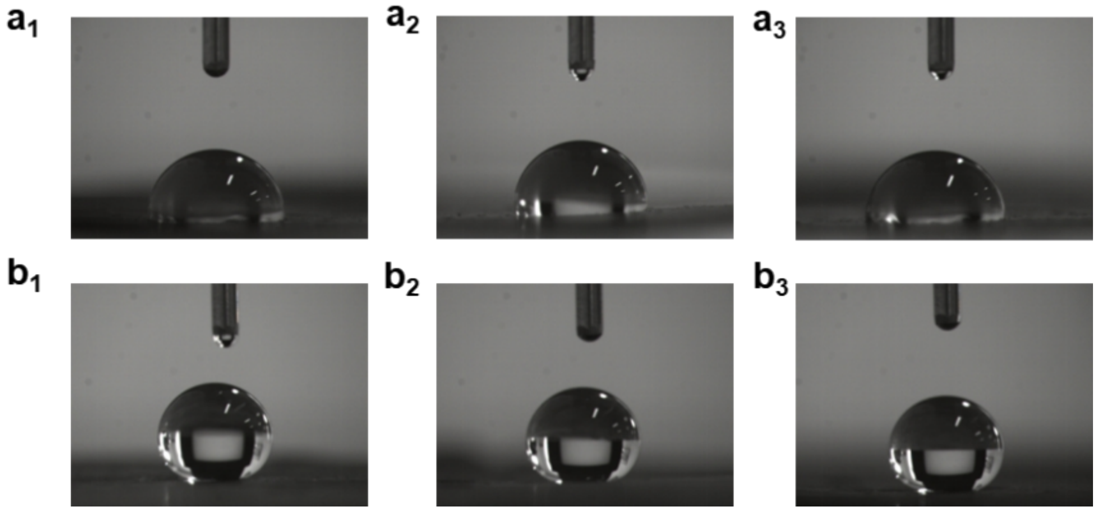

Fig. S12 Contact angle test on the film **(a_1, a_2, a_3)** before, **(b_1, b_2, b_3)** after the hydrophilic modification.

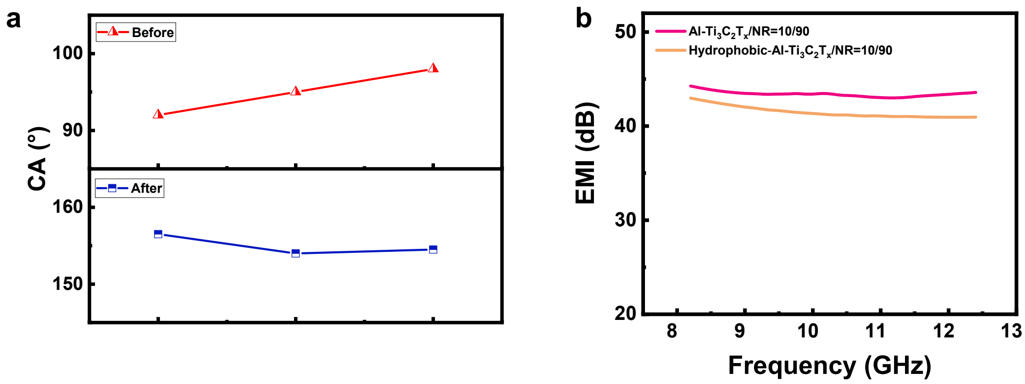

Fig. S13 Contact angle **a** and EMI **b** before and after hydrophobic modification.

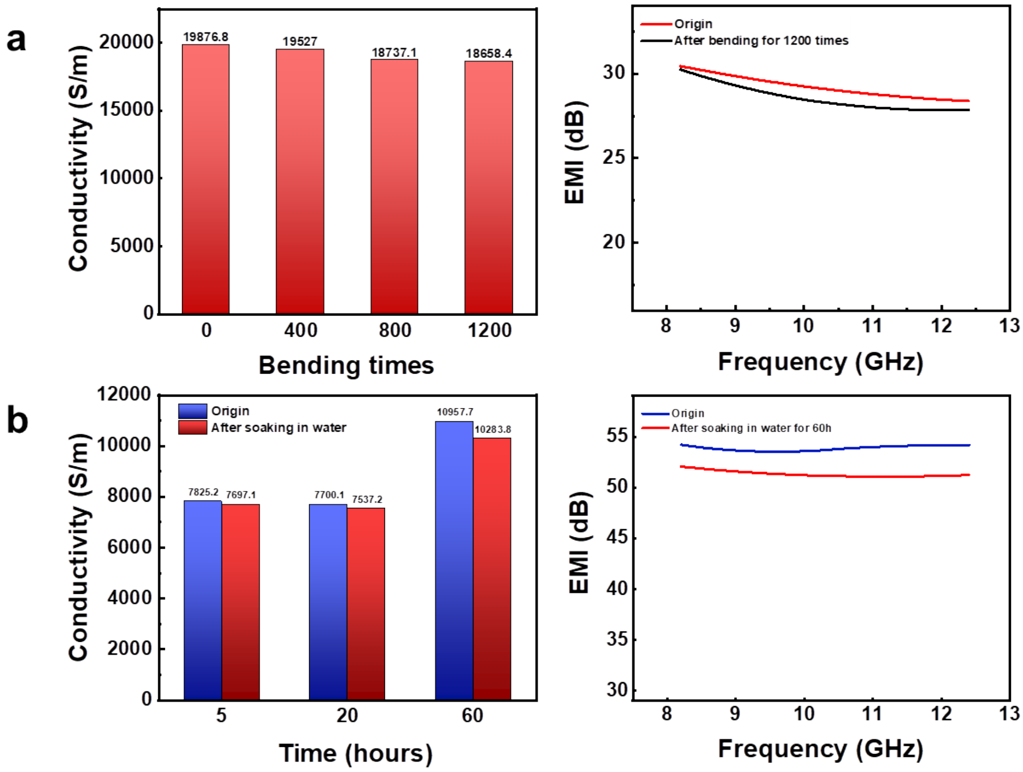

Fig. S14 Electrical conductivity and electromagnetic interference (EMI) shielding performance of the composite film under (**a**) mechanical bending cycles and (**b**) water immersion conditions.

Table S1. Comparison of the mechanical performance of MXene/NR composite films with other MXene-based composite materials.

Material	Stress (MPa)	Strain (%)	Ref
13.8 wt% PIF/MXene	21.72	11.24	20
20 wt% MXene/cellulose	11.5	4	21
6 wt% MXene/EPDM	3.06	285	22
NRMF-3	0.55	689	23
MXene/NR	34	4.5	24
Fe3O4@$Ti_3C_2T_x$/DENR-10	14.15	675	25
PRT/HENR	4.93	1042	26
6 wt% S-MXene/S-ENR	4.55	388	27
SBR-Ti_3C_2	9.05	461	28
NRMX-0.6	7.33	863.1	29
AMTE	21.57	880.06	32
MR7	18.2	761	30
FMNC-3.2	17.5	610	31
10 wt% Al-$Ti_3C_2T_x$/NR	**25.4**	**511.5**	**This Work**

Table S2. Mechanical and EMI properties of MXene/NR composite films.

Sample	Tensile Strength (MPa)	Elongation at break (%)	Tensile modulus (MPa)	Toughness (MJ/m^3)	EMI SE (dB)
Al-$Ti_3C_2T_x$/NR=0/100	12.6	1059.1	0.22	31.21	0
Al-$Ti_3C_2T_x$/NR=5/95	22.0	641.3	1.448	74.21	55
Al-$Ti_3C_2T_x$/NR=10/90	25.4	511.5	4.59	83.25	73
Al-$Ti_3C_2T_x$/NR=15/85	13.1	20.3	0.905	2.18	81
Al-$Ti_3C_2T_x$/NR=20/80	18.4	8.4	2.98	0.89	90

Al-$Ti_3C_2T_x$/NR=25/75	16.3	2.8	5.71	0.48	95
$Ti_3C_2T_x$/NR=10/90	20.15	470.34	1.66	52.73	41

Table S3. Comparison of the EMI shielding performance of MXene/NR composite films with other EMI composite materials.

Types	Materials	Thickness (mm)	EMI (dB)	SSE/t (dB cm^2 g^{-1})	Ref.
CNT-based	CNTs/PC	2.1	39	164	7
	MWCNTs/PS	2	30	285	8
	SWCNTs/PS	1.2	18.5	275	9
	MWCNTs/ABS	1.1	40	318	10
	CNTs/Cellulose	0.15	35	1372	11
	MWCNT-based composite paper	0.6	56	3583	12
Metal-based	CF /Ni/PC	0.31	72.7	1376	2
	Ni filaments	2.85	87	164.9	1
	Ni fiber/PES	2.85	58	108.7	
Graphene -based	Graphene/PDMS	1	20	3	13
	Graphene/PS	2	29	258	14
	Graphene/PMMA	2.4	19	100	15
	Graphene/PI	0.8	17-21	848	16
rGO-based	rGO/PDMS	1	30	5000	13
	rGO/PEI	2.3	12.8	191	17
	rGO/PS	2.5	45.1	692	6
	rGO/PMMA	0.24	19	1042	15
	rGO/PEDOT	0.8	70	841	18
	Aligned rGO/epoxy	0.1	38	3530	19
All carbon materials	Carbon foam	0.2	40	1250	3
	CNF mat	0.29	52.2	1362	4
	CNT/Graphene	1	26-28	2143	5

	rGO	2.5	45.1	692	6
MXene/NR	MXene/NR=5/95	0.12	55	4608	**This work**
	MXene/NR=10/90	**0.12**	**73**	**6115.6**	
	MXene/NR=15/85	0.12	81	6786	
	MXene/NR=20/80	0.127	90	7539	
	MXene/NR=25/75	0.131	95	7958.7	

Supplementary References

[1] F. Shahzad, M. Alhabeb, C.B. Hatter, B. Anasori, S.M. Hong, C.M. Koo, Y. Gogotsi, Electromagnetic interference shielding with 2D transition metal carbides (MXenes), Science, 2016, 353(6304), 1137-1140, DOI: 10.1126/science.aag2421.

[2] D. Xing, L. Lu, K.S. Teh, Z. Wan, Y. Xie, Y. Tang, Highly flexible and ultra-thin Ni-plated carbon-fabric/polycarbonate film for enhanced electromagnetic interference shielding, Carbon, 2018, 132, 32-41, DOI: 10.1016/j.carbon.2018.02.015.

[3] F. Moglie, D. Micheli, S. Laurenzi, M. Marchetti, V.M. Primiani, Electromagnetic shielding performance of carbon foams, Carbon, 2012, 50(5), 1972-1980, DOI: 10.1016/j.carbon.2011.12.053.

[4] X. Hong, D. Chung, Carbon nanofiber mats for electromagnetic interference shielding, Carbon, 2017, 111, 529-537, DOI: 10.1016/j.carbon.2016.10.026.

[5] W.-L. Song, J. Wang, L.-Z. Fan, Y. Li, C.-Y. Wang, M.-S. Cao, Interfacial engineering of carbon nanofiber–graphene–carbon nanofiber heterojunctions in flexible lightweight electromagnetic shielding networks, ACS Appl. Mater. Interfaces, 2014, 6(13), 10516-10523, DOI: 10.1021/am502103u.

[6] D.X. Yan, H. Pang, B. Li, R. Vajtai, L. Xu, P.G. Ren, J.H. Wang, Z.M. Li, Structured reduced graphene oxide/polymer composites for ultra‐efficient electromagnetic interference shielding, Adv. Funct. Mater., 2015, 25(4), 559-566, DOI: 10.1002/adfm.201403809.

[7] S. Pande, A. Chaudhary, D. Patel, B.P. Singh, R.B. Mathur, Mechanical and electrical properties of multiwall carbon nanotube/polycarbonate composites for electrostatic discharge and electromagnetic interference shielding applications, RSC Adv., 2014, 4(27), 13839-13849, DOI: 10.1039/C3RA47719A.

[8] M. Arjmand, T. Apperley, M. Okoniewski, U. Sundararaj, Comparative study of electromagnetic interference shielding properties of injection molded versus compression molded multi-walled carbon nanotube/polystyrene composites, Carbon, 2012, 50(14), 5126-5134, DOI: 10.1016/j.carbon.2012.06.052.

[9] Y. Yang, M.C. Gupta, K.L. Dudley, R.W. Lawrence, Novel carbon nanotube−polystyrene foam composites for electromagnetic interference shielding, Nano Lett., 2005, 5(11), 2131-2134, DOI: 10.1021/nl051375r.

[10] M.H. Al-Saleh, W.H. Saadeh, U. Sundararaj, EMI shielding effectiveness of carbon based nanostructured polymeric materials: a comparative study, Carbon, 2013, 60, 146-156, DOI: 10.1016/j.carbon.2013.04.008.

[11] L.-Q. Zhang, B. Yang, J. Teng, J. Lei, D.-X. Yan, G.-J. Zhong, Z.-M. Li, Tunable electromagnetic interference shielding effectiveness via multilayer assembly of regenerated cellulose as a supporting substrate and carbon nanotubes/polymer as a functional layer, J. Mater. Chem. C, 2017, 5(12), 3130-3138, DOI: 10.1039/C6TC05348A.

[12] A. Chaudhary, S. Kumari, R. Kumar, S. Teotia, B.P. Singh, A.P. Singh, S. Dhawan, S.R. Dhakate, Lightweight and easily foldable MCMB-MWCNTs composite paper with exceptional electromagnetic interference shielding, ACS Appl. Mater. Interfaces, 2016, 8(16), 10600-10608, DOI: 10.1021/acsami.6b00761.
[13] Z. Chen, C. Xu, C. Ma, W. Ren, H.M. Cheng, Lightweight and flexible graphene foam composites for high‐performance electromagnetic interference shielding, Adv. Mater., 2013, 25(9), 1296-1300, DOI: 10.1002/adma.201204196.
[14] D.-X. Yan, P.-G. Ren, H. Pang, Q. Fu, M.-B. Yang, Z.-M. Li, Efficient electromagnetic interference shielding of lightweight graphene/polystyrene composite, J. Mater. Chem., 2012, 22(36), 18772-18774, DOI: 10.1039/C2JM32692B.
[15] H.-B. Zhang, Q. Yan, W.-G. Zheng, Z. He, Z.-Z. Yu, Tough graphene－polymer microcellular foams for electromagnetic interference shielding, ACS Appl. Mater. Interfaces, 2011, 3(3), 918-924, DOI: 10.1021/am200021v.
[16] Y. Li, X. Pei, B. Shen, W. Zhai, L. Zhang, W. Zheng, Polyimide/graphene composite foam sheets with ultrahigh thermostability for electromagnetic interference shielding, RSC Adv., 2015, 5(31), 24342-24351, DOI: 10.1039/c4ra16421k.
[17] J. Ling, W. Zhai, W. Feng, B. Shen, J. Zhang, W.G. Zheng, Facile preparation of lightweight microcellular polyetherimide/graphene composite foams for electromagnetic interference shielding, ACS Appl. Mater. Interfaces, 2013, 5(7), 2677-2684, DOI: 10.1021/am303289m.
[18] N. Agnihotri, K. Chakrabarti, A. De, Highly efficient electromagnetic interference shielding using graphite nanoplatelet/poly (3, 4-ethylenedioxythiophene)–poly (styrenesulfonate) composites with enhanced thermal conductivity, RSC Adv., 2015, 5(54), 43765-43771, DOI: 10.1039/c4ra15674a.
[19] N. Yousefi, X. Sun, X. Lin, X. Shen, J. Jia, B. Zhang, B. Tang, M. Chan, J.K. Kim, Highly aligned graphene/polymer nanocomposites with excellent dielectric properties for high‐performance electromagnetic interference shielding, Adv. Mater., 2014, 26(31), 5480-5487, DOI: 10.1002/adma.201305293.
[20] K. Sun, F. Wang, W. Yang, H. Liu, C. Pan, Z. Guo, C. Liu, C. Shen, Flexible conductive polyimide fiber/MXene composite film for electromagnetic interference shielding and joule heating with excellent harsh environment tolerance, ACS Appl. Mater. Interfaces, 2021, 13(42), 50368-50380, DOI: 10.1021/acsami.1c12549.
[21] M. Zhu, X. Yan, H. Xu, Y. Xu, L. Kong, Highly conductive and flexible bilayered MXene/cellulose paper sheet for efficient electromagnetic interference

shielding applications, Ceram. Int., 2021, 47(12), 17234-17244, DOI: 10.1016/j.ceramint.2021.03.041.
[22] S. Lu, B. Li, K. Ma, S. Wang, X. Liu, Z. Ma, L. Lin, G. Zhou, D. Zhang, Flexible MXene/EPDM rubber with excellent thermal conductivity and electromagnetic interference performance, Appl. Phys. A, 2020, 126(7), 513, DOI: 10.1007/s00339-019-3210-8.
[23] Y.-D. Yang, G.-X. Liu, Y.-C. Wei, S. Liao, M.-C. Luo, Natural rubber latex/MXene foam with robust and multifunctional properties, e-Polymers, 2021, 21(1), 179-185, DOI: 10.1515/epoly-2021-0021.
[24] W. Yang, J.-J. Liu, L.-L. Wang, W. Wang, A.C.Y. Yuen, S. Peng, B. Yu, H.-D. Lu, G.H. Yeoh, C.-H. Wang, Multifunctional MXene/natural rubber composite films with exceptional flexibility and durability, Compos. Part B Eng., 2020, 188, 107875, DOI: 10.1016/j.compositesb.2020.107875.
[25] Q. Song, B. Chen, Z. Zhou, C. Lu, Flexible, stretchable and magnetic Fe3O4@ $Ti_3C_2T_x$/elastomer with supramolecular interfacial crosslinking for enhancing mechanical and electromagnetic interference shielding performance, Sci. China Mater., 2021, 64(6), 1437-1448, DOI: 10.1007/s40843-020-1548-1.
[26] Q. Gan, L. Song, Y. Wang, Q. Yuan, W. Huang, Y. Zhu, Y. Huang, Y. Song, Towards flexible and healable strain sensors via a modulated interface between Ti_3C_2 MXene and epoxidized natural rubber, Nano Energy, 2024, 120, 109141, DOI: 10.1016/j.nanoen.2023.109141.
[27] Q. Guo, X. Zhang, F. Zhao, Q. Song, G. Su, Y. Tan, Q. Tao, T. Zhou, Y. Yu, Z. Zhou, Protein-inspired self-healable Ti_3C_2 MXenes/rubber-based supramolecular elastomer for intelligent sensing, ACS Nano, 2020, 14(3), 2788-2797, DOI: 10.1021/acsnano.9b08408.
[28] Z. Jia, W. Zhang, B. Tang, S. Zhu, M. Liu, B. Zhong, Y. Luo, F. Liu, D. Jia, L. Kong, Rational design for enhancing mechanical and conductive properties of Ti_3C_2 MXene based elastomer composites, Compos. Commun., 2021, 25, 100725, DOI: 10.1016/j.coco.2021.100725.
[29] I. Wijesinghe, S. Wimalachandra, H. Chathuranga, Y. Kondarage, C.D. Hettige Dharmasiri, K.L. Firestein, T. Tesfamichael, R. Bai, Z. Lei, C. Yan, $Ti_3C_2T_x$ MXene‐Reinforced Natural Rubber Nanocomposites with Tailored Mechanical and Antiaging Properties, Adv. Eng. Mater., 2024, 26(12), 2400286, DOI: 10.1002/adem.202400286.
[30] J.-Q. Luo, S. Zhao, H.-B. Zhang, Z. Deng, L. Li, Z.-Z. Yu, Flexible, stretchable and electrically conductive MXene/natural rubber nanocomposite films for efficient electromagnetic interference shielding, Compos. Sci. Technol., 2019, 182, 107754, DOI: 10.1016/j.compscitech.2019.107754.
[31] Z. Ye, D. Zhao, F. Liu, J. Luo, X. Liu, W. Zhao, Flexible and highly conductive $Ti_3C_2T_x$/natural rubber composites with interconnected networks for high-performance electromagnetic interference shielding, Compos. Part A Appl. Sci. Manuf., 2024, 180, 108067, DOI: 10.1016/j.compositesa.2024.108067.

[32] T. Zhang, X. Li, Y. Chen, Y. Ye, Y. Chen, Q. Tang, L. Yang, G. Chang, Y. Huang, Flexible and mechanically enhanced MXene-based composite film via interfacial cation–π interactions for durable electromagnetic interference shielding, Nano Res., 2024, DOI: 10.1007/s12274-024-6533-5.